WIDE AREA, FINE RESOLUTION SAR FROM MULTI-APERTURE RADAR ARRAYS

James M. Stiles[(1)] and Nathan A. Goodman[(2)]

(1) Radar Systems and Remote Sensing Laboratory
The University of Kansas
2335 Irving Hill Road, Lawrence, Kansas 66045 USA
Phone: 1-785-864-7744, Fax: 1-785-864-7789
Email: jstiles@rsl.ku.edu

(2) Department of Electrical & Computer Engineering
The University of Arizona
1230 E. Speedway Blvd., Tucson, Arizona 85721 USA
Phone: 1-520-621-4462, Fax: 1-520-626-3144
Email: goodman@ece.arizona.edu

ABSTRACT

Wideband Multi-static radar provides scattering observations over frequency, time, and space, thus allowing for measurements in delay, Doppler, and angle-of–arrival (i.e., spatial frequency). Stationary targets ambiguous in delay and/or Doppler cannot be physically collocated, so that their spatial responses will not generally be ambiguous or even significantly correlated. As a result, a multi-static radar can be designed such that the sensor space-time-frequency ambiguity function produces no large (e.g., grating) lobes over a large illuminated area. The size of this "unambiguous" imaging area is dependent on the number of spatial apertures implemented in the wide band design, increasing in size as the number of spatial elements is increased.

The constraint on this design is the value of the measurement clutter rank, as compared to the sensor measurement dimension. Essentially, the number of illuminated resolution cells cannot exceed the number of independent measured samples. Additional spatial elements (apertures) can increase the measurement dimension without affecting clutter rank. If a sufficient number of spatial elements are available, a SAR image can be formed for a distributed target of any clutter rank (i.e., resolution and image area). It can be shown that a necessary condition is that the total aperture area must exceed the minimum aperture area condition imposed on traditional (single aperture) SAR. However, in a multi-aperture design, this total area does not determine, or limit, the extent of the illuminated area. The size of each individual element sets the illumination area, and thus adding spatial elements to a multi-static SAR design will generally improve sensor performance, without altering the illumination area or resolution size.

For contiguous spatial arrays, we find that SAR images can be formed by simply extending traditional correlation processing over space and time. For sparse, random arrays, we find that SAR image formation requires a MMSE (i.e., Wiener) estimator. The computational cost of this linear estimator can be reduced by either implementing a reduced rank version, or by applying an iterative Wiener processor (i.e. a Kalman filter). For all these SAR processors, we find that image quality improves as the number of spatial elements is increased.

1. INTRODUCTION

Recently, there has been significant interest in the possibility of constructing a "distributed" space-borne sensor from a collection of individual small satellites [1-3]. It has been shown that a cluster of satellites will remain grouped together in orbit, providing they are placed in specific geometries. The resulting "formation flying" of these satellites provides interesting opportunities in remote sensing, as this cluster of satellites would essentially form one large sensor with tremendous spatial extent (e.g., hundreds of meters to kilometers). For example, a collection of individual radar satellites could be clustered to effectively produce a single radar with a very large, albeit sparse, array [4-7]. Several research questions arise from this notion. How can the individual radars be combined to produce an optimal overall sensor? What would the performance benefits of this sensor be, in terms of both SAR and Moving Target Indication (MTI)? How should the signal processing be performed?

The benefit of a multiple satellite radar sensor is two-fold. First, the large spatial extent of the "virtual" satellite provides excellent angle-of-arrival information about an illuminated area. For example, the sensor would provide multiple baselines for interferometric processing. Secondly, multiple radar satellites, each with a coherent receiver, greatly increase the amount of independent data collected over a given time. As more satellites (i.e., receivers) are added to the array, more independent information about the illuminated area can be collected. This paper will show that, if properly processed, this information can be used to produce fine-resolution SAR images over an arbitrarily large area or swathwidth. However, traditional matched filter approaches to SAR image formation will typically not provide adequate SAR imaging results. Instead, it will be shown that a Weiner filter approach is necessary to process the space-time measurements of a multi-aperture SAR system.

2. THE RADAR MEASUREMENT MODEL

In this section, a mathematical model describing the space-time measurements of a multi-aperture SAR sensor is presented. This model will be used to develop the SAR processors presented in the remaining sections. The narrow-band, complex measurement of a SAR aperture at spatial location $\overline{r}$ and at time *t* can be expressed as:

$$\begin{aligned} r(\overline{r},t) &= \int_A \int_V \int_T \gamma_0(\overline{x})\, h(\overline{x};\overline{r},t;\overline{r}',t')\, s(\overline{r}',t')\, dt' d\overline{r}' d\overline{x} + n(\overline{r},t) \\ &= \int_A \gamma_0(\overline{x})\, \rho(\overline{x};\overline{r},t)\, d\overline{x} + n(\overline{r},t) \end{aligned} \tag{1}$$

In this representation, $s(\overline{r},t)$ describes the transmitted signal, which for a multi-aperture case can be a non-separable function space and time. The function $h(\overline{x};\overline{r},t;\overline{r}',t')$ effectively defines the measurement space-time impulse response for a point target located at $\overline{x}$ on the illuminated surface A. This function includes the transmitter and receiver responses, as well as the propagation from the transmitter (at $\overline{r}',t'$), to target, and back to the receiver (at $\overline{r},t$). Note that because of SAR motion, this impulse response is not time-invariant. The function $\gamma_0(\overline{x})$ is a normalized scattering parameter that defines the complex scattering of the distributed target across the illuminated surface A, and $n(\overline{r},t)$ is receiver noise. After evaluating the integration over all transmitter time *T* and spatial volume *V*, the response $r(\overline{r},t)$ can likewise be described as the second equation in (1). In this expression, the received signal can be viewed as a superposition of the responses from each point of the illuminated surface ($\rho(\overline{x};\overline{r},t)$), weighted by the complex scattering amplitude of the surface ($\gamma_0(\overline{x})$).

Since the complex transmit signal $s(\overline{r},t)$ will be constrained (approximately) in both time and frequency, we can accurately express the transmit signal in terms of a finite number of space-time basis functions $\varphi_n(\overline{r},t)$:

$$s(\overline{r},t) \cong \sum_n^N s_n\, \varphi_n(\overline{r},t) \tag{2}$$

Thus, the space-time transmit code is completely specified by an N dimensional data vector $\mathbf{s}$, whose elements consist of the N complex values s_n. Additionally, the scattering of the distributed target can be described as the scattering from a collection of *I* discrete scatterers, each with a complex scattering coefficient of $\gamma_i = \gamma_0(\overline{x}_i)\Delta A$, where ΔA defines a section of surface area that is less than or equal to the resolution of the radar. To accurately represent the radar measurement, the area ΔA of each surface cell must be small enough such that the number of illuminated cells *I* exceeds the clutter rank of the radar measurement. Clutter rank is approximately equal to the number of resolution cells illuminated by the radar, and thus the area ΔA, must be less than or equal to the SAR resolution on the surface [8].

As a result of these approximations, the integration of (1) can be written in a linear algebraic form:

$$\begin{aligned}\mathbf{r} &= \sum_i \gamma_i \mathbf{H}_i \mathbf{s} + \mathbf{n} \\ &= \sum_i \gamma_i \boldsymbol{\rho}_i + \mathbf{n}\end{aligned} \tag{3}$$

The vectors **r** and **n** are *M*-dimensional vectors whose elements are the space and time sampled values of $r(\overline{r},t)$ and $n(\overline{r},t)$ respectively. Essentially, the vector **r** contains the complex sampled data collected by a multi-aperture radar over time T. The elements of matrix $\mathbf{H}_i$ are:

$$H_{mn}^{i} = \int_V \int_T h(\overline{x}_i;\overline{r}_m,t_m;\overline{r}',t')\,\varphi_n(\overline{r}',t')dt'd\overline{r}' \tag{4}$$

It is important to note that since the impulse response $h(\overline{x};\overline{r},t;\overline{r}',t')$ is time-variant, the matrix $\mathbf{H}_i$ is not circulant.

The vector $\boldsymbol{\rho}_i = \mathbf{H}_i\mathbf{s}$ is the normalized space-time response of the clutter target at surface location $\overline{x}_i$, and equation (3) again shows that radar measurement is modeled as weighted superposition of responses from dissimilar targets. This is more concisely written by forming an *I* dimensional vector $\boldsymbol{\gamma}$ of elements γ_i, and a *M* by *I* matrix $\mathbf{P}$ whose columns consist of vectors $\boldsymbol{\rho}_i$:

$$\mathbf{r} = \mathbf{P}\boldsymbol{\gamma} + \mathbf{n} \tag{5}$$

where $\boldsymbol{\gamma} = \begin{bmatrix}\gamma_1 & \gamma_2 & \cdots & \gamma_I\end{bmatrix}^T$ and $\mathbf{P} = \begin{bmatrix}\boldsymbol{\rho}_1 & \boldsymbol{\rho}_2 & \cdots & \boldsymbol{\rho}_I\end{bmatrix}$. In addition to being more amenable to numeric computation, the benefit of this representation is that linear algebraic techniques can be directly applied to the radar estimation problem.

3. SINGLE-APERTURE SAR IMAGE FORMATION

Given that the radar parameters (e.g., position, velocity, wavelength, transmit signal, antenna pattern) are accurately known, the normalized target response vectors $\boldsymbol{\rho}_i$ (and therefore matrix **P)** are know *a priori*. It is surface scattering, described by complex vector $\boldsymbol{\gamma}$ that is unknown, and thus the SAR problem can be simply stated as estimating the vector $\boldsymbol{\gamma}$, given some measurement vector **r**. This paper is concerned with determining effective linear estimators, and any linear estimation process can be written as a multiplication of **r** with matrix **W**, so that **W** is regarded as the linear estimator:

$$\hat{\boldsymbol{\gamma}} = \mathbf{W}\mathbf{r} \tag{6}$$

where $\hat{\boldsymbol{\gamma}}$ is the estimate of vector $\boldsymbol{\gamma}$. Note the row vectors of matrix **W** (defined as $\mathbf{w}_i$) provide a linear estimator for each surface clutter cell (i.e., SAR pixel). An estimate of the scattering coefficient from the *i*-th surface target can thus be found by taking the inner product of $\mathbf{w}_i$ and the measured vector **r**:

$$\hat{\gamma}_i = \mathbf{w}_i^{\dagger}\mathbf{r} \tag{7}$$

It is evident from (6) that a necessary condition for providing an independent estimate of $\boldsymbol{\gamma}$ is that the dimension of **r** must meet or exceed that of $\boldsymbol{\gamma}$ ($M > I$). In other words, the number of independent measurements must exceed the clutter rank (number of illuminated resolution cells). It is this fact that ultimately limits the size of a standard SAR

image. As the illumination area is increased, the clutter rank increases until it surpasses the measurement dimension M—the result is the minimum aperture requirement for SAR sensors.

The simplest and perhaps most common linear estimator is a correlation processor, also known as a matched filter. The weight vectors $\mathbf{w}_i$ of this linear estimator are given as:

$$\mathbf{w}_i = \frac{\boldsymbol{\rho}_i}{\left|\boldsymbol{\rho}_i\right|^2} \tag{8}$$

Recall that the elements of these vectors are complex measurements across space and time, and thus (6) describes a space-time matched filter. Generally speaking, this weight vector can be separated into two independent operations, one spatial (i.e., beamforming) and one temporal (i.e., standard time-frequency SAR processing).

As a test case, a standard spaceborne SAR scenario—using one antenna element—was derived and used to calculate the values of matrix $\mathbf{P}$ (i.e., every $\boldsymbol{\rho}_i$). A flat Earth approximation was used, and the distribution of scatterers across an illuminated section of the surface was assumed to correspond to the image in Fig. 1. Each pixel of the image corresponds to an equivalently located i-th resolution cell on the surface, and the magnitude of the pixel was used to specify the magnitude of the complex scattering coefficient γ_i. The phase of each γ_i was randomly selected over 2π radians.

Fig. 1. Image representing the magnitude of the scattering across an illuminated surface, for purposes of the simulations presented in this paper

The resulting measurement vector $\mathbf{r}$ was calculated, along with a random vector $\mathbf{n}$, to specify the system noise. This measurement vector was processed with (6) to generate the SAR image of Fig. 2a. The image is obviously of poor quality, a result that was predictable since in the illuminated area in this scenario was too large (i.e., the SAR aperture was too small), so that the clutter rank greatly exceeded the measurement dimension is the minimum aperture size required by SAR. If the illumination area is decreased (the aperture is increased) to a sufficiently large value, an unambiguous image can be created, as shown in Fig. 2b. The problem with this image, of course, is that it does not cover the spatial extent of the original problem, as the larger SAR aperture illuminates a smaller region of the Earth's surface.

From this perspective, it would appear that the solution to creating an unambiguous image over the entire spatial extent represented by Fig. 1 is to increase the dimension of $\mathbf{r}$; i.e., to take more independent measurements. The dimension of $\mathbf{r}$ (assuming each measurement is independent) is equal to the time-bandwidth product (BT) of the received signal, where bandwidth B is approximately equal to the bandwidth of the transmitted signal, and T is aperture time, or Coherent Processing Interval (CPI). Increasing either of these two parameters would indeed result in more independent measurements, and therefore a larger unambiguous SAR image could be constructed. The problem is that this image

would be larger in terms of number of resolution cells, but not in spatial extent. Increasing signal bandwidth and processing time also improves range and Doppler resolution respectively. Therefore, an image of equal size but with finer resolution can be constructed, but not one of greater spatial extent. Again, the result is the well-known limit on SAR image area (e.g., swathwidth).

(a)

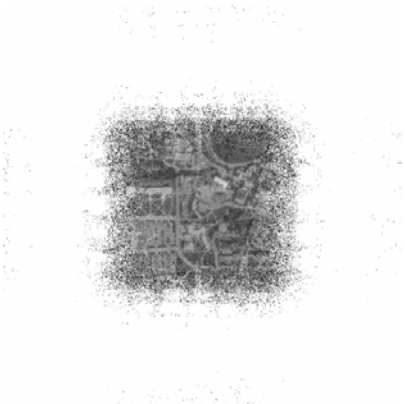

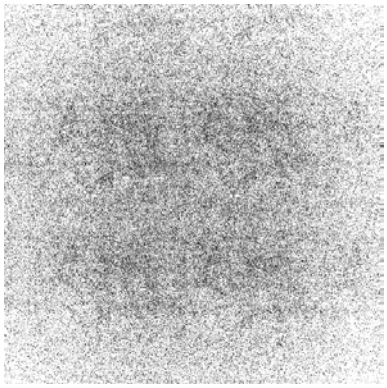

(b)

Fig. 2. The ambiguous SAR image resulting when exceeding the maximum illuminated area limit (a), and when constraining the illumination to create an unambiguous, but spatially small image (b). Both a large and unambiguous image is desired.

4. MULTI-APERTURE SAR IMAGE FORMATION

The solution, therefore, to constructing a fine-resolution SAR image over a large spatial extent is to increase the number of independent samples collected by the sensor, without modifying the resolution of the radar. In other words, the measurement must be increased without changing the measurement clutter rank. Since sensor resolution is determined by temporal (i.e., delay and Doppler) information, it is evident that additional *spatial* information can be used to increase the dimension of measured vector **r**, while preserving the fundamental resolution of the radar. For example, if the aperture used to produce the unambiguous image of Fig. 2b is subdivided to create an array of nine elements, and each element is implemented with a coherent receiver, then the number of independent measurements collected increases nine times. The elements of the radar receive vector **r** are now measurements in space and time, rather than time alone. As a result, the dimension of **r** increases as a factor of N to approximately NBT, where N is the number of elements in the array (for this case N=9).

With this additional spatial information, an unambiguous image can be formed over the entire spatial extent of the original scenario, with the result provided in Fig. 3. Correlation processing was likewise used for this example, but now this correlation was performed over measurements in space-time, rather than on time data alone. This processing effectively performs both standard delay-Doppler processing of the data across time and spatial beamforming processing of the array information.

Fig 3. Image resulting from the simulated measurements of a multi-aperture SAR. Space-time correlation processing was used, essentially providing both delay-Doppler and spatial beamforming processing.

This point is emphasized by Fig. 4. Say the image of Fig. 1 is replaced with a surface consisting of a single scattering target, placed precisely at the center of the illuminated area. Fig. 4a displays the resulting image if a single receive aperture were implemented, showing clearly the locations of the eight targets ambiguous in delay and doppler. Effectively, this image displays the ambiguity (or point spread) function of the sensor, projected onto the illuminated surface. Alternatively, Fig. 4b displays the image if only the spatial data of the nine-element array were used. This image essentially displays the array beamforming pattern, projected onto the image area. Clearly, the resolution associated with this pattern is poor compared to delay-Doppler. However, note that the main lobe is sufficiently narrow to reject the delay-Doppler ambiguous targets shown in Fig. 4a. As a result, the image created from processing the entire space-time measurement vector **r** is displayed in Fig. 4c. Effectively, this is the ambiguity function of the overall imaging sensor, a response that approaches the ideal "thumbtack" function. Note this space-time ambiguity function is effectively the multiplication of the delay-Doppler function with the spatial beamforming function. The result shows that the responses from targets in the illuminated area can be correlated in delay-Doppler, provided that they are uncorrelated spatially (and vice versa).

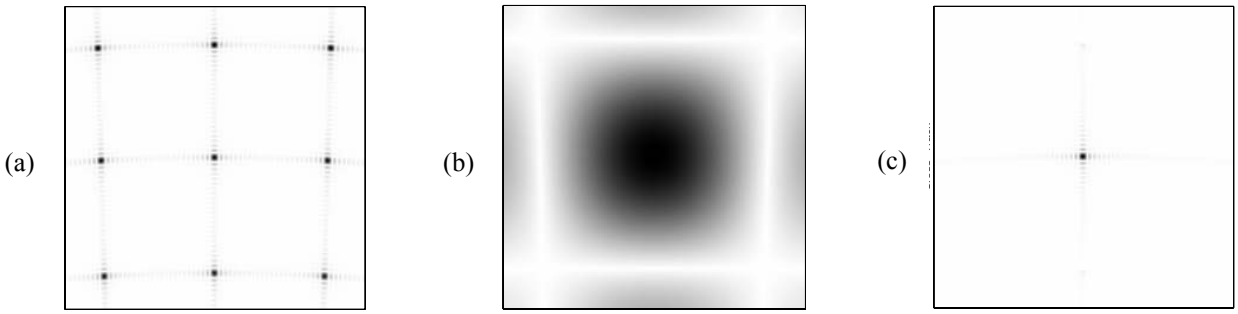

Fig. 4. The sensor delay-Doppler ambiguity function (a), the sensor spatial ambiguity function (i.e., beamforming pattern) (b), and the combined space-time ambiguity function (c).

It should be noted that a Multi-Aperture SAR (M-SAR) still retains the minimum aperture area requirement that is associated with standard SAR. If the total aperture area is too small, the beamwidth of the beamforming pattern is insufficiently narrow to reject targets ambiguous in delay-Doppler. The difference between M-SAR and standard SAR is that this limit on aperture area does not likewise limit, or otherwise determine, the size of the illuminated area or the extent of the resulting image. For any sensor resolution, an image or swathwidth of arbitrarily large extent may be obtained by subdividing the original aperture (with sufficient area) into increasingly smaller (and thus more numerous) aperture elements.

5. SPARSE MULTI-APERTURE SAR IMAGE FORMATION

For the distributed radar concept, the spatial array (i.e., satellite constellation) would be randomly and sparsely populated, as opposed to the contiguous array case considered in the previous section. A sparse array scenario was thus developed, with the relative element position randomly selected over a constrained area. Initially, space-time correlation processing was applied to the simulated measurements, with the result shown in Fig. 5.

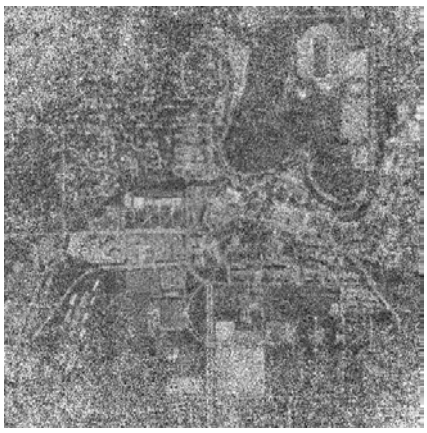

Fig. 5. A poor quality SAR image resulting from a sparse, multi-aperture SAR, using correlation processing.

Clearly, correlation processing is insufficient for forming quality SAR images with sparse spatial arrays. The reason for this is seen when examining the beamforming pattern of the sparse array, as shown in Fig. 6a. Although the large spatial extent of the array provides a narrow main beam, the sparse nature of the array leads to a pattern with significant sidelobes. The resulting space-time ambiguity function is displayed in Fig. 6b, and demonstrates that the center target is partially correlated with other targets within the illuminated area. As a result, the SAR image is of poor quality.
Another way of demonstrating this problem is to directly evaluate (6) for the matched filter case (7). The resulting estimate of γ_i is:

$$\hat{\gamma}_i = \gamma_i + \sum_{i \neq j} \gamma_j \frac{\boldsymbol{\rho}_i^{\dagger} \boldsymbol{\rho}_j}{|\boldsymbol{\rho}_i|^2} + \frac{\boldsymbol{\rho}_i^{\dagger} \mathbf{n}}{|\boldsymbol{\rho}_i|^2} \tag{9}$$

Note this estimate consists of three terms. The first is the correct scattering value γ_i ; therefore the remaining two terms represent estimate error. The last term represents error due to noise. The correlation processor minimizes this term, by maximizing the received energy with respect to noise. The second term represents error due to the correlation of the weight vector with all other illuminated targets. The correlation filter does nothing to minimize this term, and therefore, if the responses from the illuminated targets are significantly correlated, a correspondingly large error will result. Generally, for the sparse array case, the responses of some resolution cells will be significantly correlated, and thus a different linear estimator must be implemented.

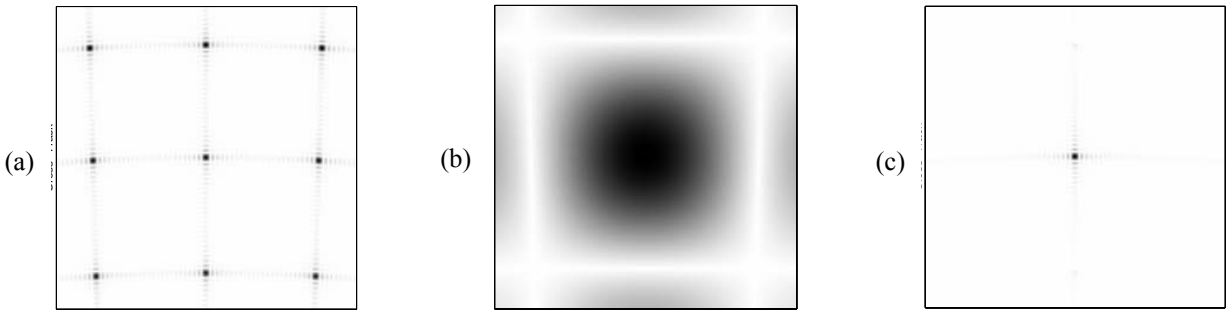

Fig 6. The beamforming pattern created by the sparse spatial array (a), and the poor space-time ambiguity function that results from this (b).

4.1 The Maximum Likelihood Estimator

The Maximum Likelihood (ML) estimator provides the estimate of $\boldsymbol{\gamma}$ that maximizes the likelihood function $p(\mathbf{r}|\boldsymbol{\gamma})$, where $p(\mathbf{r}|\boldsymbol{\gamma})$ is the conditional probability density function (pdf) of $\mathbf{r}$ given $\boldsymbol{\gamma}$. For equation (3), it can be shown that this estimate is achieved by implementing the linear estimator:

$$\mathbf{W}_{ml} = \mathbf{P}^{\sim 1} \tag{10}$$

where $\mathbf{P}^{\sim 1}$ is the pseudo inverse of matrix $\mathbf{P}$. The ML estimator provides a weight vector $\mathbf{w}_i$ that is orthogonal to all other illuminated targets (i.e., $\mathbf{w}_i^{\dagger} \boldsymbol{\rho}_{j \neq i} = 0$). Essentially, the ML estimator correlates $\mathbf{r}$ with the component of the target vector $\boldsymbol{\rho}_i$ that resides in a subspace orthogonal to the responses of all other resolution cells. Thus, this estimator minimizes the error due to clutter, where clutter is defined as the responses from all other resolution cells.

There are, however, two requirements for satisfactory results when implementing the ML estimator. The first is that the matrix $\mathbf{P}$ be well conditioned, so that that the inverse $\mathbf{P}^{\sim 1}$ can be effectively determined. This requirement can generally be satisfied if the dimension of $\mathbf{r}$ far exceeds the measurement clutter rank. In other words, the requirement can be satisfied if the number of apertures in the sparse array significantly exceeds the minimum required for proper image formation. The second requirement relates to system noise. The ML estimator minimizes the estimate error due to clutter, but does nothing to minimize the error due to noise. As a result, the estimate error (i.e., the SAR image) quickly degrades as measurement SNR declines.

4.2 The Minimum Mean-Squared Error Estimator

Given that we have some *a priori* knowledge of the radar SNR, a minimum mean-squared error estimator can be implemented, which can be shown to be:

$$\mathbf{W}_{mmse} = \sigma_\gamma^2 \mathbf{P}' \left[\mathbf{P}\mathbf{P}' \sigma_\gamma^2 + \sigma_n^2 \mathbf{I} \right]^{-1} \tag{11}$$

where σ_γ^2 is the expected value of $|\gamma_i|^2$, and σ_n^2 is the expected value of $|n_k|^2$, where n_k is a element of noise vector **n**. It can be shown that this solution is likewise the Maximum A Posteriori (MAP) estimator, which is the solution that maximizes the function $p(\boldsymbol{\gamma}|\mathbf{r})$, where $p(\boldsymbol{\gamma}|\mathbf{r})$ is the conditional pdf of $\boldsymbol{\gamma}$ given **r**. . The resulting imaging is displayed in Fig. 7, and demonstrates a marked improvement over the correlation processor of Fig. 5. The simulation data used in both Figs. 5 and 7 are identical, the only difference between the results were the linear estimators used to process that data.

Fig. 7. A quality SAR image resulting from a sparse, multi-aperture SAR, using MMSE processing.

This estimator is the discrete implementation of a Wiener filter and minimizes the estimation error due to both noise and clutter. In other words, if the correlation processor maximizes signal to noise, and the ML estimator maximizes signal to clutter, the MMSE estimator can be said to maximize signal to interference, where interference is defined as the summation of both clutter and noise energy. Accordingly, this estimator provides SAR images superior to both correlation and ML processing for all SNR. It should be likewise noted that the ML and MMSE estimators are true space-time solutions, in that the resulting weight vectors are not separable in space and time. In contrast to the correlation processor, these solutions cannot be viewed or interpreted as a time-frequency Wiener filter followed by a spatial Wiener filter.

The cost of implementing this processing is the additional complexity in determining the linear estimator $\mathbf{W}_{mmse}$. However, it should be noted that once $\mathbf{W}_{mmse}$ is calculated, the basic matrix multiplication $\mathbf{W}_{mmse}$ **r** is no more complex than either the correlation or the ML estimator. Additionally, for large problems, the matrix inverse operation can be problematic. Reduced rank methods can be implemented [9], a technique used to produce all the results in this paper. The time data at each receiver were processed with a matched filter, and then the ML and MMSE processing was completed on the remaining spatial data. In this manner, the rank of the matrices to be inverted was no greater than the number of array elements, typically less than 20.

An alternative approach is to apply an iterative solution of the Wiener filter [10], commonly known as the Kalman filter. For this implementation, the measurement data vector **r** is first sub-divided into multiple segments. The innovation vector and Kalman gain is determined for each measurement segment, and the SAR image estimate is updated. When all the data segment of vector **r** are used, the resulting image is identical to the Wiener (MMSE) solution applied to the entire measurement vector **r**. The benefit in implementing the iterative (i.e., Kalman) solution is strictly computational efficiency, as the Kalman gain calculation requires an inversion of a matrix whose dimension is equal to the dimension

of each data segment. The result is that the MMSE SAR image is formed by determining the inverse of many small matrices, as opposed to one large matrix inversion. The result is significant computational savings, particularly when the dimension of the measurement data vector **r** is very large.

6. ERROR ANALYSIS

A number of simulations were conducted for various sensor scenarios to evaluate the performance of the various processing techniques as a function of measurement SNR and number of receiver apertures. The evaluation criterion was the mean-squared error of the scattering values γ_i, as compared to the actual values displayed by Fig. 1. Fig. 8 displays this error as a function of the number of receive apertures used by the sensor. For each case, a sparse aperture design was implemented, wherein the positions of the apertures were randomly selected within a constrained region. A minimum of nine apertures was required to collect a sufficient number of independent samples for this test case, so the horizontal axis of Fig. 8 begins at nine.

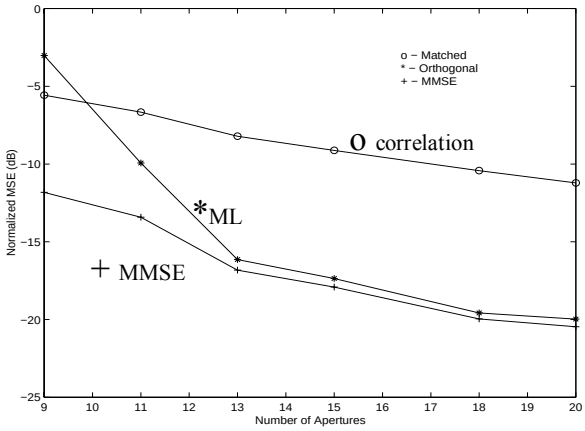

Fig. 8. SAR image error as a function of number of receiver elements. The best results occur when the number of elements significantly exceeds the minimum number required for image formation.

Fig. 8 shows that image quality for all three processors improves as the number of receivers increases, with particularly sharp improvement in the ML and MMSE results. As stated earlier, extending the number of receive apertures beyond the required minimum improves the condition of the matrix that must inverted, and thus improves the resulting image from MMSE and, particularly, ML estimation. Fig. 9 displays the performance of the estimators as a function of SNR. The SNR value presented is the SNR of a single radar measurement; in other words, the average SNR of a single element in vector **r.** The figure demonstrates the superiority of the MMSE processor at all SNR. It likewise shows the sensitivity of the ML to SNR, approaching MMSE performance as SNR increases, but degrading rapidly as SNR decreases. Finally, the plot demonstrates that, unlike the ML or MMSE estimator, the correlation processor is not an efficient estimator. In other words, the estimation error associated with the correlation processor does not converge to zero as SNR approaches infinity.

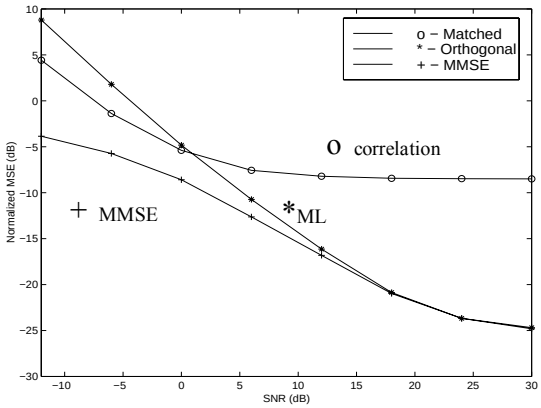

Fig. 9. SAR image error as a function of measurement SNR. Note the MMSE processor provides the best results for all SNR.

7. CONCLUSIONS

The idea of a distributed, multi-aperture spaceborne sensor represents a new paradigm for SAR sensor design. The strength of this idea is the addition of a wide volume of spatial samples to the traditional delay-Doppler SAR information. Although the resulting spatial array is sparse and random, the resulting spatial data is sufficient to decorrelate surface target responses that are otherwise perfectly correlated (ambiguous) in delay and Doppler. As a result, a sufficiently populated multi-aperture sensor can be used to form unambiguous, fine-resolution SAR images over a wide surface area or swathwidth. However, image formation can be accomplished only by implementation of a space-time Weiner filter, as opposed to the traditional correlation processing used in standard SAR sensors.

ACKNOWLEDGEMENT

This worked was funded by the US Air Force Office of Scientific Research (AFOSR), grant # AFOSR F49620-99-1-0172.

REFERENCES

1. Zetocha P., et al, "Commanding and controlling satellite clusters," *IEEE Intelligent Systems*, vol. 15, no. 6, pp. 8-13, Nov., 2000.
2. Kitts C., et al, "Emerald: a low-cost spacecraft mission for validating formation flying technologies," *Proc. 1999 IEEE Aerospace Conf.*, Aspen, CO, pp. 217-226.
3. Yedavalli, R.K., Sparks, A.G.; "Satellite formation flying control design based on hybrid control system stability analysis," *Proc. 2000American Control Conference*, Vol. 3, 2210-2214, 2000.
4. Massonnet D., et al, "A wheel of passive radar microsats for upgrading existing SAR projects," *Proc. IEEE 2000 Int. Geosci. Rem. Sens. Symp.*, Honolulu, HI, 1000-1003.
5. Massonnet D., "Capabilities and limitations of the interferometric cartwheel," *IEEE Trans. Geosci. Rem. Sens.*, vol. 39, no. 3, 506-520, 2001.
6. Goodman N., Lin S.C., Rajakrishna D., and Stiles J.M., "Processing of multiple receiver, spaceborne arrays for wide-area SAR," *IEEE Transactions on Geoscience and Remote Sensing,* vol. 40, 841-852, 2002.
7. Das A., Cobb R., and Stallard M., "TechSat 21: a revolutionary concept in distributed space based sensing," *Proc. of the AIAA Defense and Civil Space Programs Conference and Exhibit*, Huntsville, AL, AIAA 98-5255, 1998.
8. Goodman N. and Stiles J.M., "Synthetic Aperture Characterization of Radar Satellite Constellations," in *Proceedings of the IEEE International Geoscience and Remote Sensing Symposium,* vol. 1, 665-667, 2002.
9. Honig M.L. and Xiao W., "Performance of reduced-rank linear interference suppression," vol. 47, no. 5, 1928-1946, 2001.
10. Kay S.M., *Fundamentals of Statistical Signal Processing: Estimation Theory*, Prentice Hall, Saddle River, NJ, 1993.